

Ultraefficient on-Chip Supercontinuum Generation from Sign-Alternating-Dispersion Waveguides

Haider Zia,* Kaixuan Ye, Yvan Klaver, David Marpaung, and Klaus-Jochen Boller

Fully integrated supercontinuum sources on-chip are critical to enabling applications such as portable and mechanically stable medical imaging devices, chemical sensing, and light detection and ranging. However, the low efficiency of current supercontinuum generation schemes prevents full on-chip integration. Herein, a scheme where the input energy requirements for integrated supercontinuum generation are drastically lowered by orders of magnitude is presented, for bandwidth generation of the order of 500–1000 nm. Through sign-alternating dispersion in a CMOS-compatible silicon nitride waveguide, an efficiency enhancement by factors reaching 2800 is achieved. It is shown that the pulse energy requirement for large-bandwidth supercontinuum generation at high spectral power (e.g., 1/e level) is lowered from nanojoules to 6 picojoules. The lowered pulse energy requirements enable that chip-integrated laser sources, such as mode-locked heterogeneously or hybrid-integrated diode lasers, can be used as a pump source, enabling fully integrated on-chip high-bandwidth supercontinuum sources.

1. Introduction

Significantly increasing bandwidth through intensity-dependent nonlinearity, that is, supercontinuum generation (SCG),^[1–3] is central to a vast plethora of applications such as in frequency combs,^[4,5] hyperspectral light detection and ranging (LiDAR),^[6,7] optical coherence tomography (OCT),^[8,9] or nonlinear optical pulse compression.^[10,11] Most implementations of SCG require significant pump-pulse energy to broaden the

spectral bandwidth at useful power levels for most applications.^[12] Achieving ultra-wide bandwidth spectra remains challenging with on-chip pump sources due to the high pulse energy requirements, thereby limiting full integration of laser sources on chip with SCG waveguides.

Currently, chip-scale SCG^[13,14] requires pump-pulse energies in the order of hundreds of picojoules or several nanojoules. However, pumping SCG with chip-integrated laser sources, such as with mode-locked heterogeneously or hybrid-integrated diode lasers,^[15,16] would require that the SCG can be achieved with significantly lower pulse energies in the sub-10 pJ, presenting a major bottleneck in achieving compact SCG sources. The low-pulse-energy requirement especially limits bandwidth generation within the high spectral power 1/e (≈ -4 dB) range, crucial


for interferometric applications such as OCT and the generation of ultrashort pulses.

Nowadays several approaches have been explored to lower this pump energy requirement. One approach is to utilize materials with a smaller bandgap, which increases a waveguide's effective nonlinear coefficient via increased nonlinear susceptibility.^[17,18] However, this may limit material choices for efficient nonlinear bandwidth generation. Another method relies on enhancing the peak intensity by tightly confining the optical radiation within the waveguide. Thus, choosing a high-index contrast waveguide CMOS-compatible platform, such as silicon nitride circuits, further increases the peak intensity and bandwidth.^[19,20] These methods eventually fall through because the pulse's peak power is lost or rendered ineffective by the interaction of waveguide dispersion and self-phase modulation. Due to dispersion, either temporal broadening will occur, reducing peak power, or the pulse forms into stationary solitons, both leading to stagnation of spectral generation above the -20 dB range.^[21] Thus, simply increasing the confinement or increasing the waveguide length is not effective in matching the low-pulse-energy requirements of fully integrated SCG sources.

A promising approach is to alternate the sign of dispersion in segments of different lengths across the propagation to counteract both types of SCG stagnation mechanisms of spectral generation.^[22,23] The bandwidth increase, notably at the 1/e level, is then ongoing with increasing number of alternating dispersion segments, resulting in a substantially increased spectral generation length, terminating only if waveguide losses start to dominate.

H. Zia, K.-J. Boller
Department Science & Technology
Laser Physics and Nonlinear Optics Group
MESA+ Research Institute for Nanotechnology
University of Twente
7500 Enschede, AE, The Netherlands
E-mail: h.zia@superlightphotonics.com

K. Ye, Y. Klaver, D. Marpaung
Department Science & Technology
Nonlinear Nanophotonics Group
MESA+ Research Institute for Nanotechnology
University of Twente
7500 Enschede, AE, The Netherlands

 The ORCID identification number(s) for the author(s) of this article can be found under <https://doi.org/10.1002/adpr.202200296>.

© 2023 The Authors. Advanced Photonics Research published by Wiley-VCH GmbH. This is an open access article under the terms of the Creative Commons Attribution License, which permits use, distribution and reproduction in any medium, provided the original work is properly cited.

DOI: 10.1002/adpr.202200296

In this letter, we report novel implementations to increase spectral generation efficiency of the bandwidth at high spectral power, needed for applications such as OCTs or nonlinear pulse compression in integrated waveguide SCGs.^[24] We experimentally demonstrate SCG generation in repeatedly sign-alternated dispersion silicon nitride waveguides, which exhibits 1/e bandwidth generation enhancement up to 2800 times compared to the state-of-the-art. The increased energy efficiency of our approach leads to required pulse energy down to the sub-10 pJ level. Our results represent an important step toward all-integrated wide-bandwidth portable light sources.

2. Results

2.1. Design of the Alternating Dispersion Waveguides

A conceptual illustration of the alternating waveguides is shown in **Figure 1a**. In our waveguide design of fixed thickness, step-wise variation of the waveguide width along the propagation direction is used to set the dispersion at normal dispersion (ND) or anomalous dispersion (AD).

Due to alternating dispersion, the loss of peak power from temporal broadening in ND is offset by pulse compression in AD segments. In turn, the cessation of spectral generation due to soliton formation^[25] in anomalous segments is overcome by spectral generation in the ND segments and by nonlinear compression of the chirped stretched pulse in the subsequent AD segments. The spectral generation then remains across a longer interaction length of the waveguide, resulting in large spectral enhancements of SCG by sign alternation of dispersion.

To minimize losses, adiabatic tapers are placed to connect the segments in a chain. The pulse compression to shorter durations per subsequent AD segment and the increasing frequency chirp and duration after the ND segments are indicated in the figure by the colored example profiles of the pulse's electric field profile after some of the segments.

As shown in **Figure 1a** (not to scale), two alternating structures are considered to maximize spectral bandwidth to pump-power efficiency for either the vertical or horizontal input linear polarization state. Structure 1 maximizes the spectral generation of the mode with vertical polarization (s), while structure 2 maximizes that of horizontal polarization (p). Structure 1 has more width iterations than structure 2.

The two structures were designed using an SCG solver,^[23] based on the nonlinear Schrödinger equation, described in the Experimental Section. The structures were fabricated at the Ligentec foundry with losses of less than 0.05 dB cm⁻¹ by use of SiN/SiO high-resolution all-nitride (AN) technology^[26] (see Experimental Section and Supporting Information I on the structures, solver, and losses).

The calculated dispersion spectra of the AD and ND segments are compared in **Figure 1b,c** for both s and p-polarizations. The shaded areas indicate the bandwidth across which the sign of the dispersion is inverted, which is ≈ 750 nm for s-polarization, covering a wavelength range from 1200 to 1950 nm. The inversion bandwidth for p-polarization is 300 nm with wavelength range from 1300 to 1600 nm. The expectation is that the generated bandwidth spans at least the sign inversion wavelength

range, where dispersive loss of peak intensity and soliton formation are prevented.

The experimental setup is shown in **Figure 1d** and described in Experimental Section. An input pulse centered at 1554 nm, with 21 nm bandwidth and an approximate duration of 165 fs, was used from an ultrafast fiber laser (Toptica FemtoFiber Ultra). Pulses were coupled into the waveguides through a lensed fiber (pulse duration after lensed fiber is 179 fs, with negligible nonlinearity, shown in Experimental Section).

2.2. Low-Pulse-Energy Spectral Output of the Alternating Dispersion Waveguides

The output power spectra were measured at different pulse energies and polarization states for each waveguide structure. The overall transmission loss through the waveguide circuits was calculated using the loss values provided by the manufacturer as given in the Supporting Information I. To determine the in-coupled power independent of uncertainties in mode-matching efficiencies at the input, the power in the waveguides was measured at the output and corrected for propagation loss. Using manufacturer provided values and simulations, we estimate that losses due to propagation and outcoupling do not exceed a maximum total of 30%. In order to effectively compare the simulations with experiment, we refer to the estimated pulse energy just after incoupling to the waveguide.

Figure 2a shows the output spectral power plotted against wavelength for structure 1 for the s-polarized input. With increasing pulse energy, both the bandwidth increases and the amount of spectral power approaching or exceeding the 1/e level. However, of main importance is that the structures provide an unprecedented bandwidth generated at low pulse energy. The high bandwidth efficiency reveals itself by the low pulse energy threshold, needed for the 1/e width to exceed the sign-inversion dispersion bandwidth (marked in yellow in **Figure 2a**) at 34 pJ (24 pJ measured after the output lens).

At the threshold pulse energy at 34 pJ, the bandwidth spans from ≈ 1500 to 2450 nm, that is, 950 nm. At the -30 dB level, the spectrum spans more than an octave. As pulse energy increases, the spectrum flattens within the 1/e width which in turn increases to greater than 1000 nm at an output pulse energy of 55 pJ. Increasing pulse energy also results in narrowband dispersive wave components at ≈ 480 , 515, and 550 nm, shown in the inset.

An example spectrum obtained from our solver is shown as the dotted curve in **Figure 2a**. While the simulated spectrum has a pulse energy of 20 pJ, it best matches the experiment at pulse energy of 34 pJ in terms of profile and bandwidth. The offset is likely from remaining deviations between the assumed numerical dispersion profiles and nonlinear coefficients and the actual profiles obtained from the fabrication process. However, while these deviations are present, as can be seen from the experiments, the simulation was able to still find an efficient sign-alternating dispersion structure that maximizes the 1/e bandwidth range, describes the salient dispersive and nonlinear effects, and shows the expected shape of the spectral profile.

As shown in **Figure 2a,b**, it was experimentally found that for both structures, the spectral bandwidth exceeds the

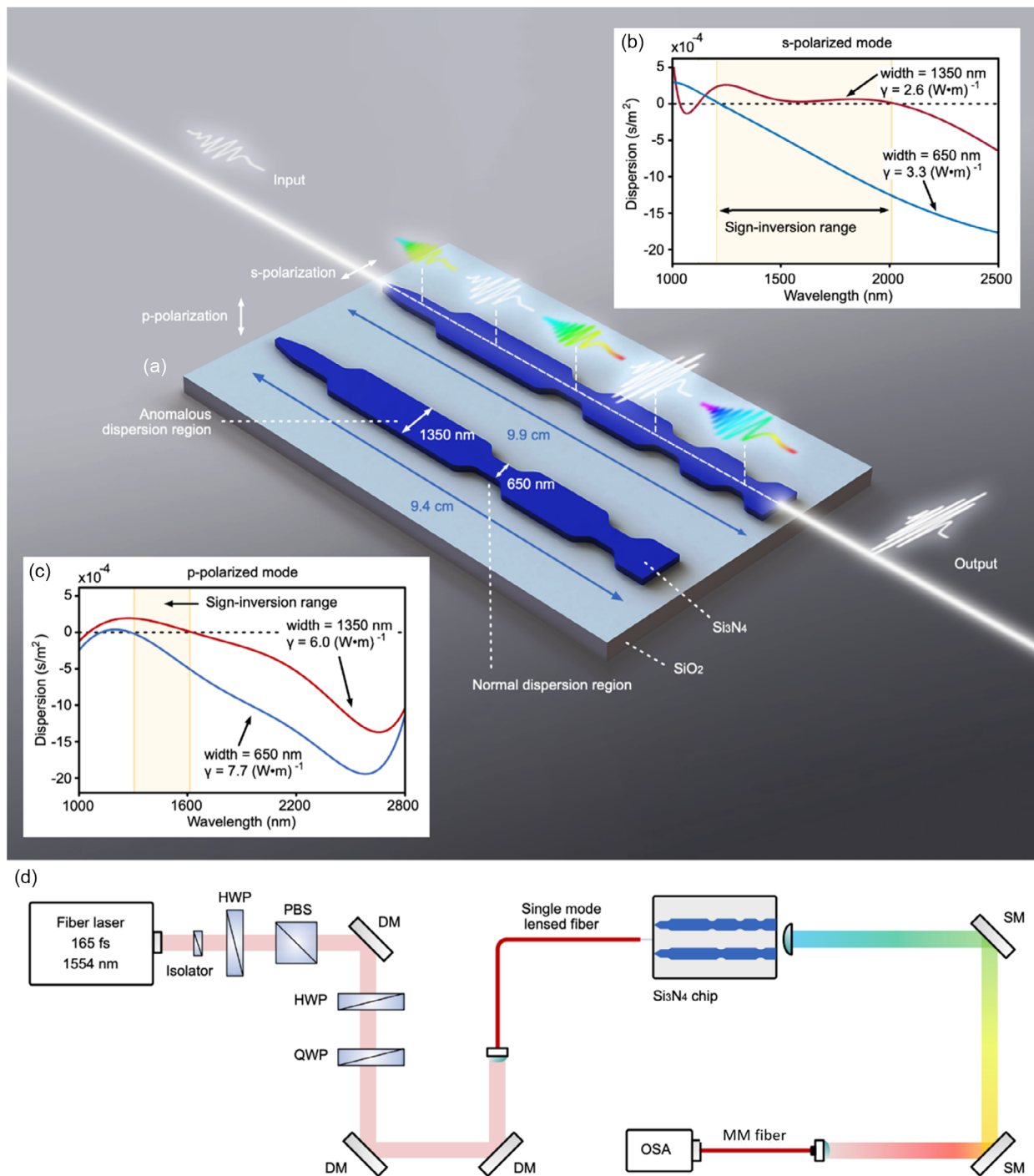


Figure 1. Sign-alternated-dispersion silicon nitride waveguides for efficient SCG. a) An illustration of integrated waveguide structure 1 and structure 2. The darker region indicates the silicon nitride core, while the lighter region corresponds to the silicon oxide cladding. The overall lengths of both structures are indicated, and the amounts of ND and AD segments are also shown. Nonlinear pulse propagation is shown through the qualitative dynamics of the illustrated electric field profiles. The length and width of the segments are not shown to scale. For the exact geometrical dimensions of the waveguides, refer to Supporting Information I. b) Calculated dispersion profiles of the s-polarized mode versus wavelength for the AD segment of 1350 nm width (shown in red) and the ND segment of 650 nm width (shown in blue). The associated nonlinear coefficients of the waveguides are indicated as well. The shaded region is the wavelength range where the sign of dispersion is inverted. c) Dispersion profiles for p-polarizations, analogous to panel (b). d) Illustration of the experimental setup. A fiber laser delivering ultrashort pulses was used as the source. PBS refers to polarization beam splitter, DM refers to dielectric mirror (1550 nm), SM to broadband silver mirror, and MM refers to multi-mode fiber. Optical spectrum analyzer (OSA) refers to near-infrared or visible range optical spectrum analyzers (Ocean View NirQuest256 and Ando AQ6315A spectrum analyzer).

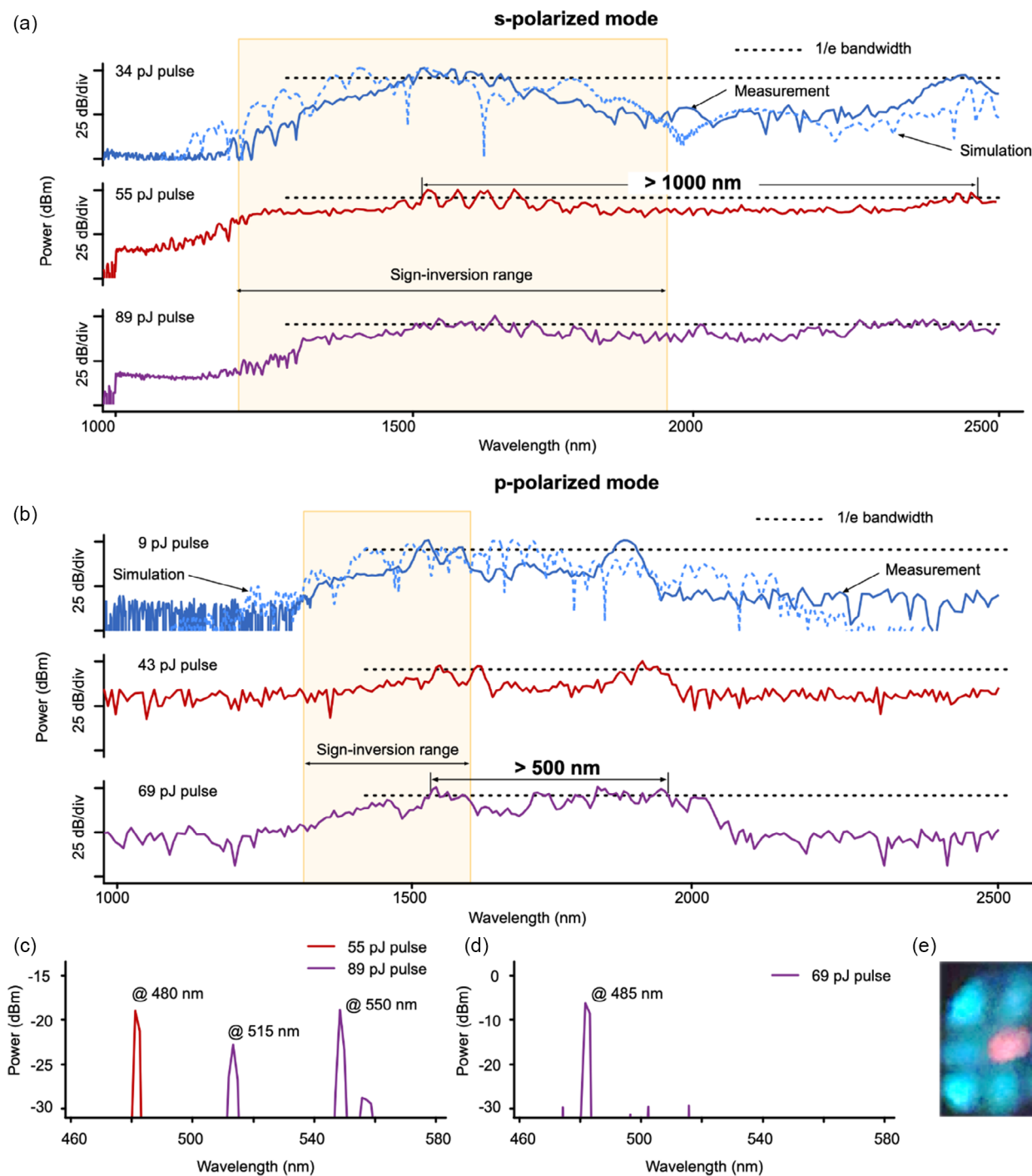


Figure 2. Measured supercontinuum spectra from the silicon nitride waveguides. a) Spectral power versus wavelength on a logarithmic scale for structure 1's s-polarization mode, recorded at stepwise increased pulse energies as indicated in plots. Dispersive waves in the visible range are indicated in the inset. b) Same plot as for (a) for structure 2's p-polarization mode. c) Spectral power of the visible dispersive waves of structure 1 at a pulse energy of 55 and 89 pJ. d) Spectral power of the visible dispersive waves of structure 2 at a pulse energy of 69 pJ. e) Real-color image of an example of higher-order modes of the visible dispersive wave at 485 nm. The pink coloring in the center is due to the IR sensitivity of the camera.

sign-inversion wavelength range. We first explain this finding, to supplement the above discussion on the nonlinear pulse dynamics in sign-alternating dispersion structures.

As confirmed by simulations, the efficient spectral bandwidth generated outside the inversion region is from dispersive waves generated in the AD and ND segments as follows. As the optical

pulse repeatedly undergoes spectral generation in subsequent AD and ND segments, dispersive waves are also repeatedly generated. However, the main pulse profile changes (e.g., in peak intensity) due to the nonlinear propagation within each segment, generating a different frequency profile of dispersive waves at each segment. The superposition of all the generated dispersive waves then creates the broadband spectral profile above the 1/e-level and outside the inversion range, seen in the output spectra (refer to Supporting Information II for more details).

In the presentation of spectra in this article, we start at the pulse energy when the formation of the broadband dispersive waves surpasses the 1/e level. However, substantial spectral broadening (e.g., >200 nm) occurs already at lower pulse energies, but with a 1/e-level bandwidth contained within the inversion wavelength range.

The total bandwidth generated is generally larger with wider inversion bandwidth, as seen when comparing s-polarization bandwidth to that of p-polarization for structure 1 and 2 respectively (Figure 2b). Structure 2 is designed to maximize the bandwidth of p-polarization, a 1/e spectral width of ≈ 375 nm is obtained at 9 pJ pulse. The simulation trace is shown as the dotted blue line. Narrowband high-power visible dispersive waves, exceeding the -20 dB level, are found between 480 and 580 nm in structure 1 (Figure 2c). For structure 2, a dispersive wave at 485 nm exceeds the -8 dB level, as shown in Figure 2d. The visible dispersive waves for structure 1 and 2 exhibit higher-order spatial modes. For example, the dispersive wave at 485 nm is approximately a TE₃₃ mode, as shown in Figure 2e.

The visible dispersive waves are in higher-order modes and thus, we surmise that they are not from the traditional self-phase modulation (SPM)–group velocity dispersion (GVD) dynamics but result from spontaneous four-wave mixing in the AD segments (i.e., they are close to the third harmonic) and then are amplified by the increased spatial overlap of the radiation in the more confined ND segments and phase matching conditions for both segments.

Additional spectra for the p-polarization for structure 1 and s-polarization for structure 2 are shown in Supporting Information III. The bandwidth and spectral profiles for the other polarizations for structure 1 and 2 are similar to the corresponding polarizations presented here, albeit occurring at higher-output pulse energies.

However, while the total bandwidth is higher for the s-polarization, due to an enlarged inversion bandwidth, we predict that p-polarization would output a better temporal profile and shorter pulse. The prediction is because the overall dispersions for a large region past 1550 nm for both the AD and ND segments are lower in absolute magnitude than for the s-polarization. The lower dispersion values also result in a flatter spectrum, as shown in the spectral output results (Figure 2b). The flatter spectrum would also yield a higher pulse compression and minimize side lobes in the temporal pulse profile.

3. Discussion

To put our results in context, we defined an efficiency enhancement factor (η_{BP}) to compare the spectral efficiency versus input pulse energy of our sign-alternated devices with other integrated

SiN SCG setups. The efficiency enhancement factor gives the gain of efficiency of our work compared to others and is given as

$$\eta_{BP} = \frac{\Delta\lambda_{alt} E_{ref}}{\Delta\lambda_{ref} E_{alt}} \quad (1)$$

In Equation (1), $\Delta\lambda$ refers to the output 1/e bandwidth and ‘E’ refers to input pulse energy. The index ‘alt’ represents alternating dispersion for our p and s-polarization structures while ‘ref’ indicates previously reported experimental data without alternation.

Equation (1) provides a means of quantifying various SCG schemes across a wide parameter range. The η_{BP} as defined should be seen with some caution as it cannot incorporate all the specifics of each case and is therefore only a global measure. On the other hand, it is independent of specific waveguide parameters, only looking at the overall efficiency of state-of-the-art systems as compared to ours.

We also note that our comparison does not factor in the relative flatness of the spectrum above the 1/e level, that is, there are dips within this bandwidth range below the 1/e level. However, the same spectral quality can be seen in the studies we compare to with large-enough bandwidth to display such dips, for example, other studies refs. [12,27–29].

We tabulate the efficiency enhancement factor of our method in comparison to several state-of-the-art experimental results for SCG in the integrated silicon nitride platform,^[12,13,27–32] shown in **Table 1** for both structure 1 (s-polarization input) and structure 2 (p-polarization input) around a central wavelength of 1550 nm. With regard to all of the compared works, the alternating SCG waveguides show a clear relative advantage for both polarizations and a maximum efficiency enhancement factor of $\eta_{BP} > 2700$.

We also tabulate our work, in **Table 2**, compared to other significant studies at largely differing central wavelengths (λ_0), for example, at 1 or >2 μm . Here we adjust the bandwidth of these studies by an approximate factor, given as $[\frac{1550\text{ nm}}{\lambda_0}]^2$ so that it can be an effective bandwidth that can be compared to our study centered at 1550 nm.

To signify the wide parameter range encompassed by the references shown in Table 1 and 2, we also include cases where alternating dispersion does not seem to offer an advantage on a first view, as the efficiency enhancement factor is comparatively low ($\eta_{BP} \approx 3$ and 12, marked by asterisks or double crosses in Table 1 and 2). However, closer inspection shows that also here there is a clear advantage, because these works used waveguides with a nonlinear refractive index and coefficient an order of magnitude higher, for example, with silicon-rich nitride (USRN: indicated by double crosses) or have nonlinear coefficients around 3 times higher (indicated by asterisks).

To compare our SiN waveguides more accurately to platforms with higher nonlinearity, it is important to obtain an equivalent pulse peak power that normalizes the waveguide nonlinear coefficients. We find that the nonlinear term in the nonlinear evolution equation scales with the peak power, that is, P_0 while it scales linearly with the waveguide nonlinear coefficient (see Experimental Section). Therefore, the pulse peak power should be adjusted by $[\frac{\gamma_1}{\gamma_0}]$ where γ_1 is the nonlinear coefficient of the study in question and γ_0 is the highest nonlinear

Table 1. Efficiency comparison to previous state-of-the-art integrated SCG sources.

Technology ^{a)}	Materials	Pump Pulse Input		SCG 1/e Bandwidth [nm]	Efficiency [nm pJ ⁻¹]	Efficiency ratio of our work to cited work	
		FWHM [fs]	Energy [pJ]				
This work: s-pol. Optimized alternating waveguide	Silicon nitride on oxide	180	34	950	28		
This work: p-pol. Optimized alternating waveguide	Silicon nitride on oxide	180	9	375	42	s-pol. Optimized alternating waveguide	p-pol. Optimized alternating waveguide
Two segment, either width or cladding removal, cascaded anomalous dispersion waveguide ^[44]	Silicon nitride on oxide, 100 nm length	60	220	83	0.4	74	110
Wide (1300 nm) uniform-width anomalous waveguide ^[13]	Silicon nitride on oxide	120	1400	21	0.02	1900	2800
Bragg grating-enhanced SCG ^{[30]x}	Silicon-rich nitride on oxide (USRN)	1700	10	24	2.4	12	17
Previous state of the art in efficiency SCG OCT source (operating at 1300 nm) ^[12]	Silicon nitride on oxide pumped at 1300 nm	200	25	110	4.4	6	9
Uncladded high-confinement anomalous dispersion waveguide ^[28]	Silicon nitride on oxide	78	300	1000	3.3	8	13
Crossphase modulation intermodal SCG ^[29]	Silicon nitride on oxide	88	250	100	0.4	70	100

^{a)}The asterisk refers to works with a waveguide nonlinear coefficient, approximately a factor of around 3 times higher than what was used in our structures. The double cross refers to a work in silicon rich nitride (USRN) with a nonlinear refractive index and coefficient approximately an order of magnitude higher than our structures. The double asterisk refers to a work with nonlinear coefficient 28 times higher than the maximum used in our structures.

Table 2. Efficiency comparison to previous state-of-the-art integrated SCG sources at central wavelength significantly different from our work.

Technology ^{a)}	Materials	Pump Pulse Input		Effective Bandwidth [nm]	Efficiency [nm pJ ⁻¹]	Efficiency ratio of our work to cited work	
		FWHM [fs]	Energy [pJ]				
This work: s-pol. Optimized alternating waveguide	silicon nitride on oxide	180	34	950	28		
This work: p-pol. Optimized alternating waveguide	silicon nitride on oxide	180	9	375	42	s-pol. Optimized alternating waveguide	p-pol. Optimized alternating waveguide
Low pulse energy SCG ^{[34]x*}	Highly nonlinear waveguides (220 Wm ⁻¹), Silicon on oxide at 2300 nm	70	4	135	34	≈1	≈1
Low pulse energy SCG ^[45]	Silicon nitride pumped at 1064 nm	70	18	11	0.6	48	71
Bragg grating and confinement-enhanced SCG ^{[27]x}	Silicon on insulator (SOI) at 1950 nm	250	27	221	8	3	5
Enhanced confinement and tapered anomalous waveguides ^{[31]x}	Silicon on insulator (SOI) pumped at 1950 nm	250	27	252	9	3	5
Uniform-width anomalous waveguide ^[32]	Silicon nitride on oxide, pumped at 1030 nm	115	590	340	0.7	49	71

^{a)}The asterisk refers to works with a waveguide nonlinear coefficient, approximately a factor of around 3 times higher than what was used in our structures. The double cross refers to a work in silicon rich nitride (USRN) with a nonlinear refractive index and coefficient approximately an order of magnitude higher than our structures. The double asterisk refers to a work with nonlinear coefficient 28 times higher than the maximum used in our structures.

coefficient of our SiN structures. In ref. [30], the comparison yields that the 1/e bandwidth at a pulse energy of ≈9 pJ would be needed in the comparison table and in ref. [27] the bandwidth at 2.7 pJ would need to be determined, to obtain an efficiency comparison neglecting the influence of the higher material nonlinearity.

Most closely matching our own pulse duration (180 fs) are the most recent experiments described in another study ref. [12]

(200 fs). In that example a state-of-the-art integrated OCT source is demonstrated, showing a spectral width of 100 nm at 25 pJ, while our approach provides a width of 950 nm using 34 pJ pulses, yielding a relative efficiency enhancement factor of $\eta_{BP} = 9$, that is, input pulse energy requirements are lowered by almost an order of magnitude. We note that this holds true when factoring the lower central wavelength of 1300 nm as opposed to 1550 nm in our study. To adjust for this wavelength

mismatch, the effective bandwidth of ref. [12] that can be compared to ours would be multiplied by $\left[\frac{1550\text{ nm}}{1300\text{ nm}}\right]^2 \approx 1.4$, yielding an adjustment of our efficiency factor from 9 to 6.

The structures in Table 1 and 2 span a length shorter than our structures. In our approach, the AD segment lengths are lower than the soliton fission length but are terminated right before soliton fission occurs. This condition ensures that spectral generation in the AD segments is maximized and that solitons would not be generated. We avoid that solitons are generated because any spectral generation is then limited but modulations in the spectrum increase, that is, the spectral quality degrades. In fact, in past soliton fission, the spectral bandwidth may even decrease in the AD segments or within the ND segments because of the temporal distribution of the soliton bunch center frequencies, that is, they have an opposite chirp profile to what generates spectrum in the SPM–GVD dynamics.^[33]

Since the soliton fission length increases at lower pulse energy, and waveguide nonlinearity, the footprint of our structures, spanning ≈ 9 cm on a 5 mm by 10 mm chip, is larger than structures considered in the table. However, the longer AD segments to utilize the full range possible for spectral generation, coupled with sign alternation, is what generates the high efficiencies recorded in Table 1 and 2 of our approach and enables large 1/e bandwidth generation at low pulse energy (see Supporting Information for more details).

In regard to past work in dispersion management for SCG, the use of complex machine learning algorithms has been explored recently in silicon on insulator where 1/e bandwidths of 300 nm, centered at 2300 nm, have been achieved at 4 pJ but through a highly nonlinear coefficient of 220 (Wm)^{-1} .^[34]

In contrast, our approach indicates that more efficient SCG 1/e bandwidth generation can take place by simply alternating the sign of dispersion, in materials with low nonlinearity (at most 8 (Wm)^{-1}). It would be of interest to compare the findings of the machine learning algorithm to our approach of sign alternation in a waveguide system with the same material nonlinearity for both methods. If sign alternation produces comparable or better efficiency, then the reduction in complexity can narrow the parameter space for SCG machine learning algorithms or obtain a better set of input constraints. We predict that with the help of machine learning algorithms, such as what is presented in another study,^[34] a more optimal design can be found where regions of AD waveguides and ND waveguides are alternately iterated, however, not necessarily at two fixed waveguide widths (with adiabatic tapers in between) as done in this study. We have outlined how such a device can be used to optimize for nonlinear temporal pulse compression in the study by Zia et al.^[23]

4. Conclusion

In conclusion, alternating dispersion waveguides for wide-bandwidth generation at the 1/e bandwidth are an important step forward for all-integrated SCG sources. Our approach can be implemented in a variety of material platforms where dispersion can be engineered by the geometry of the waveguide, that is, in high-contrast refractive index materials. For follow-up studies, we plan to extend the material platforms of our approach and

optimize the output temporal profiles of the pulses for pulse compression applications.

The pulse energy needed for wide-bandwidth SCG at the 1/e width, found to be 9 pJ at 1550 nm in our approach, is now coming into proximity with the 1–3 pJ pulse range offered by state-of-the-art integrated ultrafast diode lasers centered at 1550 nm.^[15,16] Ultrashort pulse durations are supported by the bandwidth of the laser described in ref. [16], and the required moderate upscaling of the pulse energy appears feasible, for example, with on-chip amplification.^[35]

Diode-pumped solid-state waveguide lasers are more challenging regarding CMOS compatibility although the required optical pumping has shown great progress with off-chip pump lasers. While these lasers operate so far only in the continuous wave (CW) regime,^[36] they hold potential as a laser source for the sign-alternating SCG waveguides presented in this letter, since noticeably higher upper-state lifetimes and, correspondingly, higher pulse energies are offered.

5. Experimental Section

Experimental Setup: A Toptica FemtoFiber Ultra laser was used, centered at 1554 nm, with 78 MHz repetition rate and a pulse duration of 165 fs full width at half maximum. The laser was operated at maximum power, so the output pulses had the widest spectral profile. The experimental setup is shown through the schematic in Figure 1d), in the main text.

The source pulses passed through an isolator to minimize feedback. A half-wave plate and polarization beam splitter (PBS) arrangement was then placed to serve as a variable power attenuator.

After the average power was lowered, the laser pulses were passed through another half-wave-plate and quarter-wave-plate arrangements, such that the polarization state was set to the s- or p-polarization entering the alternating waveguide downstream. The quarter-wave plate is necessary to account for the birefringence in the lensed fiber used to couple light into the waveguide.

Next, the pulses passed through a lensed fiber (OZ optics, TSMJ-3S-1550-9/125-0.25-5-5-45-0.28-POL-AR) consisting of SMF28 fiber of ≈ 30 cm in length, terminated by a taper down to a tip diameter of 5 μm . The lensed fiber maximized the power coupled into the waveguide (21%), calculated from the output power, and estimated propagation loss. The dispersive effects were then verified to be negligible by measuring the pulse duration at the output of the fiber, using an autocorrelator (APE PulseCheck NX NIR), and the autocorrelation trace is shown in Figure 3a. The associated Gaussian pulse duration at the full width half maximum (FWHM) was ≈ 179 fs, which was similar to that of the source laser (164 fs). Nonlinear effects in the fiber were verified to be negligible by measuring the spectrum of the pulses at the fiber end facet using an Ando AQ6315A spectrum analyzer (Figure 3b). Figure 3b shows the spectral power after the lensed fiber for the maximum power used into the chip compared to the spectral power before the lensed fiber.

The fiber was mounted on a five-axis stage (Nanomax Thorlabs, three translational, pitch, and yaw) to maximize input coupling. The waveguides were mounted on a separate stage with only translation perpendicular to the propagation axis. The pulses were outcoupled from the waveguides and collimated using a 3.1 mm aspheric focus lens (Thorlabs C330TMD-C) on a three-axis stage (Nanomax, Thorlabs). The near-infrared spectrum was measured using a NIR spectrometer (Ocean View NirQuest256) with range from 850 to 2500 nm. The portion of the spectrum, from 350 to 850 nm, was measured with the Ando spectrum analyzer, whose total range extended from 350 to 1750 nm.

Waveguide Design and Fabrication: The waveguide width profile versus propagation coordinate was found, by solving the associated group-velocity dispersion profile using a numerical solver (Supporting

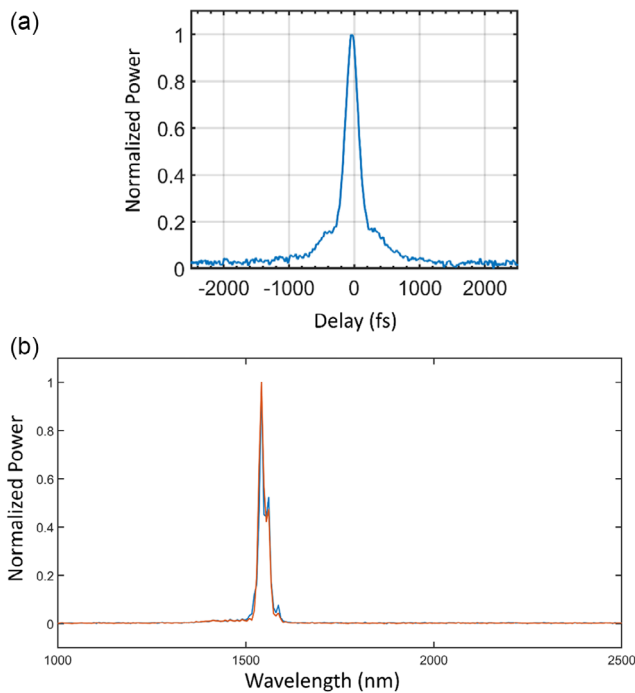


Figure 3. a) Autocorrelation trace at maximum power used for the experiment after the lensed fiber. b) Spectrum at powers used in the experiment, after the lensed fiber (blue), compared to the spectrum input into the lensed fiber (red).

Information I), and this information was the basis for the fabrication of the structure. Parameters for the waveguide, such as the inverse input taper and the adiabatic taper lengths between segments, losses, and minimal bend radii, were provided by VLC photonics. The chip layout and wafer run were designed and coordinated by VLC Photonics as well.

The fixed thickness of our waveguides was 800 nm, and the width of the ND segments was 650 nm while that of the AD segments was 1350 nm. Adiabatic tapers, with a length of 59 μm , were placed to connect the segments. Structure 1 had a total length of 9.9 cm, and Structure 2 had a length of 9.4 cm. Both had an input inverse taper starting at a core width of 200 nm. Both structures were folded on a 2 cm by 1 cm chip where the bend radii were chosen such that the bends negligibly influenced the optical radiation.

Theory of Nonlinear Pulse Propagation and SCG: The experiment was modeled using a generalized nonlinear Schrödinger equation (GNLSE) under the slowly-varying envelope approximation, given in Equation (2).^[17]

$$\frac{\partial u}{\partial z} = \sum_{k \geq 2} \frac{i^{k+1}}{k!} \beta_k \frac{\partial^k u}{\partial \tau^k} + i\gamma \left(1 + i\tau_s \frac{\partial}{\partial \tau} \right) |u|^2 u \quad (2)$$

where u is the complex field envelope and β_k is the Taylor series coefficient of the expansion of the frequency-dependent wavenumber about the central frequency, ω_0 . Since the expansion started at $k = 2$, this amounted to the Taylor series expansion of the group-velocity dispersion. $\tau = t - V_g z$ is the time coordinate, comoving in the frame of reference of the group velocity dispersion ($V_g \equiv \beta_1^{-1}$). τ_s is the characteristic timescale of self-steepening (shock time), given as ≈ 5 fs. The equation was evaluated using the split-step exponential Fourier method^[37] iteratively along the propagation coordinate z . The procedure to obtain the frequency-dependent group velocity dispersion of the segments is described in Supporting Information I.^[38–43]

To compare our approach with platforms at different waveguide nonlinearities, it was important to note the following derivation.

The material nonlinearity and the pulse peak power acted to increase the nonlinear term in the GNLSE equation, in the same way.

This can be seen by normalizing Equation (2) to the peak value of the input pulse power, that is, $P_0 = \max(|u|_0^2)$, the equation becomes

$$\frac{\partial U}{\partial z} = \sum_{k \geq 2} \frac{i^{k+1}}{k!} \beta_k \frac{\partial^k U}{\partial \tau^k} + i\gamma \left(1 + i\tau_s \frac{\partial}{\partial \tau} \right) P_0 |U|^2 U \quad (3)$$

$$U = u / \max(u_0) \quad (4)$$

The conclusion to this derivation was that the pulse peak power should be adjusted by $\left[\frac{\gamma_1}{\gamma_0} \right]$ where γ_1 is the nonlinear coefficient of the study in question and γ_0 is the highest nonlinear coefficient of our SiN structures to obtain a meaningful comparison of performance across different waveguide platforms.

Supporting Information

Supporting Information is available from the Wiley Online Library or from the author.

Acknowledgements

The authors gratefully acknowledge Toptica Photonics AG for the pulsed laser source, Ocean Insight for the NIR spectrometer, and APE GmbH for the NIR autocorrelator. The authors also acknowledge VLC Photonics and Ligentec SA for the silicon nitride chip fabrication. H.Z. would like to acknowledge funding from the NWO through the Demonstrator Grant, project number 18562.

Conflict of Interest

Haider Zia and Klaus-J. Boller are owners of: US and international patents entitled SYSTEMS, METHODS, AND STRUCTURES FOR IMPROVED SUPERCONTINUUM GENERATION. Haider Zia is founder of Superlight Photonics which provides technology that is in part based on this paper.

Data Availability Statement

The data that support the findings of this study are available from the corresponding author upon reasonable request.

Keywords

dispersion engineering, integrated photonics, silicon nitrides, supercontinuum generation, ultrafast pulses

Received: October 27, 2022

Revised: December 7, 2022

Published online:

- [1] J. M. Dudley, J. R. Taylor, *Nat. Photonics* **2009**, *3*, 85.
- [2] R. R. Alfano, *The Supercontinuum Laser Source: The Ultimate White Light*, Springer, New York, USA **2016**.
- [3] P. S. J. Russell, P. Hölzer, W. Chang, A. Abdolvand, J. C. Travers, *Nat. Photonics* **2014**, *8*, 278.
- [4] T. Udem, R. Holzwarth, T. W. Hänsch, *Nature* **2002**, *416*, 233.
- [5] B. Stern, X. Ji, Y. Okawachi, A. L. Gaeta, M. Lipson, *Nature* **2018**, *562*, 401.

- [6] Y. Jiang, S. Karpf, B. Jalali, *Nat. Photonics* **2020**, *14*, 14.
- [7] Y. Chen, E. Rääkkönen, S. Kaasalainen, J. Suomalainen, T. Hakala, J. Hyypää, R. Chen, *Sensors* **2010**, *10*, 7057.
- [8] N. M. Israelsen, C. R. Petersen, A. Barh, D. Jain, M. Jensen, G. Hanneschläger, P. Tidemand-Lichtenberg, C. Pedersen, A. Podoleanu, O. Bang, *Light Sci. Appl.* **2019**, *8*, 1.
- [9] N. Nishizawa, Y. Chen, P. Hsiung, E. P. Ippen, J. G. Fujimoto, *Opt. Lett.* **2004**, *29*, 2846.
- [10] J. C. Travers, T. F. Grigoroza, C. Brahm, F. Belli, *Nat. Photonics* **2019**, *13*, 547.
- [11] H. Chen, Z. Haider, J. Lim, S. Xu, Z. Yang, F. X. Kärtner, G. Chang, *Opt. Lett.* **2013**, *38*, 4927.
- [12] X. Ji, D. Mojahed, Y. Okawachi, A. L. Gaeta, C. P. Hendon, M. Lipson, *Sci. Adv.* **2021**, *7*, 1.
- [13] M. A. G. Porcel, F. Schepers, J. P. Epping, T. Hellwig, M. Hoekman, R. G. Heideman, P. J. M. van der Slot, C. J. Lee, R. Schmidt, R. Bratschitsch, C. Fallnich, K.-J. Boller, *Opt. Express* **2017**, *25*, 1542.
- [14] X. Liu, B. Zhou, M. Bache, C. J. Kruckel, A. Fulop, V. Torres-Company, *Opt. Lett.* **2016**, *41*, 2719.
- [15] A. Hermans, K. Van Gasse, J. Kjellman, C. Caër, T. Nakamura, Y. Inada, K. Hisada, T. Hirasawa, S. Cuyvers, S. Kumari, A. Marinins, R. Jansen, G. Roelkens, P. Soussan, X. Rottenberg, B. Kuyken, *APL Photonics* **2021**, *6*, 096102.
- [16] H. M. J. Bastiaens, G. Neijts, A. Memon, Y. Fan, J. Mak, D. Geskus, M. Hoekman, V. Moskalenko, E. A. J. M. Bente, K. J. Boller, *Opt. InfoBase Conf. Pap.* **2021**, *4*, 6654.
- [17] J. M. Dudley, G. Genty, S. Coen, *Rev. Mod. Phys.* **2006**, *78*, 1135.
- [18] A. Ishizawa, R. Kou, T. Goto, T. Tsuchizawa, N. Matsuda, K. Hitachi, T. Nishikawa, K. Yamada, T. Sogawa, H. Gotoh, *Sci. Rep.* **2017**, *7*, 1.
- [19] C. G. H. Roeloffzen, M. Hoekman, E. J. Klein, L. S. Wevers, R. B. Timens, D. Marchenko, D. Geskus, R. Dekker, A. Alippi, R. Grootjans, A. Van Rees, R. M. Oldenbeuving, J. P. Epping, R. G. Heideman, K. Worhoff, A. Leinse, D. Geuzebroek, E. Schreuder, P. W. L. Van Dijk, I. Visscher, C. Taddei, Y. Fan, C. Taballione, Y. Liu, D. Marpaung, L. Zhuang, M. Benelajla, K. J. Boller, *IEEE J. Sel. Top. Quantum Electron.* **2018**, *24*, 1.
- [20] M. H. P. Pfeiffer, J. Liu, A. S. Raja, T. Morais, B. Ghadiani, T. J. Kippenberg, *Optica* **2018**, *5*, 884.
- [21] A. M. Heidt, J. S. Feehan, J. H. V. Price, T. Feurer, *J. Opt. Soc. Am. B* **2017**, *34*, 764.
- [22] H. Zia, N. M. Lüpken, T. Hellwig, C. Fallnich, K. J. Boller, *Laser Photonics Rev.* **2020**, *14*, 2000031.
- [23] H. Zia, *Photonics* **2021**, *8*, 1.
- [24] B. Braaf, M. G. O. Gräfe, N. Uribe-Patarroyo, B. E. Bouma, B. J. Vakoc, J. F. de Boer, S. Donner, J. Weichsel, *OCT-Based Velocimetry for Blood Flow Quantification*, Springer, Cham **2019**, https://doi.org/10.1007/978-3-030-16638-0_7.
- [25] B. A. Malomed, *Soliton Management in Periodic Systems*, Springer, USA **2006**.
- [26] A. Stroganov, M. Geiselmann, in *ECIO 2019 - Eur. Conf. Integr. Opt.*, ECIO, Ghent, Belgium **2019**, pp. 1–3.
- [27] N. Singh, M. Raval, E. Ippen, M. R. Watts, F. X. Kärtner, *Appl. Phys. Lett.* **2021**, *118*, 071106.
- [28] E. Tagkoudi, C. G. Amiot, G. Genty, C. S. Brès, *Opt. Express* **2021**, *29*, 21348.
- [29] N. M. Lüpken, M. Timmerkamp, R. Scheibinger, K. Schaarschmidt, M. A. Schmidt, K. J. Boller, C. Fallnich, *Laser Photonics Rev.* **2021**, *15*, 2100125.
- [30] E. Sahin, A. Blanco-Redondo, B.-U. Sohn, Y. Cao, G. F. R. Chen, D. K. T. Ng, B. J. Eggleton, D. T. H. Tan, *Adv. Photonics Res.* **2021**, *2*, 2100107.
- [31] N. Singh, D. Vermulen, A. Ruocco, N. Li, E. Ippen, F. X. Kärtner, M. R. Watts, *Opt. Express* **2019**, *27*, 31698.
- [32] J. P. Epping, T. Hellwig, M. Hoekman, R. Mateman, A. Leinse, R. G. Heideman, A. van Rees, P. J. M. van der Slot, C. J. Lee, C. Fallnich, K.-J. Boller, *Opt. Express* **2015**, *23*, 19596.
- [33] D. A. Sidorov-Biryukov, A. Fernandez, L. Zhu, A. Pugžlys, E. E. Serebryannikov, A. Baltuška, A. M. Zheltikov, *Opt. Express* **2008**, *16*, 2502.
- [34] J. Wei, C. Ciret, M. Billet, F. Leo, B. Kuyken, S. P. Gorza, *Phys. Rev. Appl.* **2020**, *14*, 054045.
- [35] H. Zhao, S. Pinna, F. Sang, B. Song, S. T. S. Brunelli, L. A. Coldren, J. Klamkin, *IEEE J. Sel. Top. Quantum Electron.* **2019**, *25*, 1.
- [36] W. A. P. M. Hendriks, L. Chang, C. I. van Emmerik, J. Mu, M. de Goede, M. Dijkstra, S. M. Garcia-Blanco, *Adv. Phys.: X* **2021**, *6*, 1833753.
- [37] J. Hult, *J. Light. Technol.* **2007**, *25*, 3770.
- [38] K. Luke, Y. Okawachi, M. R. E. Lamont, A. L. Gaeta, M. Lipson, *Opt. Lett.* **2015**, *40*, 4823.
- [39] I. H. Malitson, *J. Opt. Soc. Am.* **1965**, *55*, 1205.
- [40] T. Bååk, *Appl. Opt.* **1982**, *21*, 1069.
- [41] H. R. Philipp, *J. Electrochem. Soc.* **1973**, *120*, 295.
- [42] D. Melati, F. Morichetti, A. Melloni, *J. Opt.* **2014**, *16*, 055502.
- [43] C. A. A. Franken, A. van Rees, L. V. Winkler, Y. Fan, D. Geskus, R. Dekker, D. H. Geuzebroek, C. Fallnich, P. J. M. van der Slot, K.-J. Boller, *Opt. Lett.* **2021**, *46*, 4904.
- [44] D. R. Carlson, P. Hutchison, D. D. Hickstein, S. B. Papp, *Opt. Express* **2019**, *27*, 37374.
- [45] A. J. Metcalf, T. Anderson, C. F. Bender, S. Blakeslee, W. Brand, D. R. Carlson, W. D. Cochran, S. A. Diddams, M. Endl, C. Fredrick, S. Halverson, D. D. Hickstein, F. Hearty, J. Jennings, S. Kanodia, K. F. Kaplan, E. Levi, E. Lubar, S. Mahadevan, A. Monson, J. P. Ninan, C. Nitroy, S. Osterman, S. B. Papp, F. Quinlan, L. Ramsey, P. Robertson, A. Roy, C. Schwab, S. Sigurdsson, et al., *Optica* **2019**, *6*, 233.